Magnetic Field Prediction of U-shaped Interior Permanent Magnet Motor Considering Magnetic Bridge Saturation

Du, Yunlu; Huang, Yunkai; Guo, Baocheng; Peng, Fei; Yao, Yu; Dong, Jianning

DOI
10.1109/TMAG.2023.3296718

Publication date
2023

Document Version
Final published version

Published in
IEEE Transactions on Magnetics

Magnetic Field Prediction of U-Shaped Interior Permanent Magnet Motor Considering Magnetic Bridge Saturation

Yunlu Du[1], Yunkai Huang[1], Baocheng Guo[2], Fei Peng[1], Yu Yao[1], and Jianning Dong[3]

[1]School of Electrical Engineering, Southeast University, Nanjing 210096, China
[2]School of Electrical and Automation Engineering, Nanjing Normal University, Nanjing 210023, China
[3]Department of Electrical Sustainable Energy, Delft University of Technology, 2628 CD Delft, The Netherlands

In this article, a new analytical model for predicting the magnetic field of the U-shaped interior permanent magnet motor (IPMM) is proposed. In the polar coordinates, rectangular permanent magnets are equivalent to the combination of consistent fan-shaped subdomains, and after that, the Laplace or Poisson equation of each solution domain can be obtained. Furthermore, based on the harmonic modeling (HM) technique, the saturation characteristics of the magnetic bridge are accurately considered, and then its magnetic field distribution (MFD) and electromagnetic performances (EPs) can be obtained. The approach proposed in this article includes but is not limited to U-shaped IPMMs, and it can also be applied to spoke-type or V-shaped IPMMs with a minor modification.

Index Terms— **Harmonic modeling (HM), magnetic bridge saturation, magnetic field, U-shaped interior permanent magnet motor (IPMM).**

I. Introduction

THE interior permanent magnet motor (IPMM) has the advantages of high power density, high torque density, and high efficiency [1]. It has been widely used in electric vehicles, electric aircraft, and household appliances. As a typical topology of IPMMs, U-shaped IPMMs have a unique structure that can provide better flux concentration performance and thus have received extensive attention from motor researchers.

The precise prediction of magnetic field distribution (MFD) serves as the foundation for the design and optimization of U-shaped IPMMs. As it can take into account the nonlinearity of ferromagnetic materials and complex geometric structures, finite element (FE) analysis is regarded as an effective analysis tool in the field of motor design. However, the modeling and analysis of FE models are usually complex and time-consuming [2]. The alternative analysis method is the analytic method. A technique of calculating the magnetic field of a U-shaped IPMM was proposed in [3], which estimated the MFD under no-load conditions, but the saturation effect is neglected. The magnetic bridge exhibits a local inhomogeneous magnetic saturation phenomenon due to the magnetic flux concentration effect of the IPMMs, and the magnetic field changes nonlinearly, making the accurate analytical calculation of the magnetic field a huge challenge. To solve the aforementioned issues, [4], [5], [6] proposed a hybrid analytical model (HAM) that takes into account the nonlinearity of ferromagnetic materials by combining the exact subdomain method (SDM) and the magnetic equivalent circuit (MEC) technique. However, in the aforementioned HAMs, the iron parts are modeled by the MEC method, and the modeling of reluctance elements undoubtedly increases the complexity of the analytical model. To solve the aforementioned issues, harmonic modeling (HM) technology based on complex Fourier series (CFS) decomposition embeds the permeability of ferromagnetic materials into the solution of the static magnetic field [7], [8]. The influence of nonlinear saturation can be considered without the utilization of additional analytical models, resulting in a novel approach for rapid and accurate computation of the magnetic field of the U-shaped IPMMs.

On the other hand, inspired by [3], the rectangular permanent magnet is simplified into a combination of fan-shaped regions, resulting in a consistent PM region in 2-D polar coordinates. Then the MFD and electromagnetic performances (EPs) can be obtained by solving the partial differential equation (PDE) of each subdomain.

In this article, a new approach taking into account magnetic bridge saturation is presented for the magnetic field computation of U-shaped IPMM by combining HM technology and an improved rectangular PM modeling method. The proposed approach can also be applied to V-shaped, or Spoke-type IPMMs.

II. Studied Machine

To illustrate the proposed analytical method proposed in this article, a 24 slot/4 pole U-shaped IPMM is studied. The initial rotor structure is shown in Fig. 1. To obtain the regular rotor calculation region in the polar coordinates, the original rotor structure needs to be simplified. Specifically, two Spoke-type rectangular PMs are equivalent to two fan-shaped PMs respectively, and a straight-shaped rectangular PM is equivalent to a fan-shaped PM, as shown in Fig. 2.

As shown in Fig. 2, the original Spoke-type PM region is replaced by two fan-shaped calculation regions (i.e., IV, V).

The width w_{fan} of each fan-shaped region is

$$w_{\text{fan}} = \frac{R_5 - R_3}{k} \tag{1}$$

Manuscript received 8 June 2023; revised 11 July 2023; accepted 15 July 2023. Date of publication 19 July 2023; date of current version 27 February 2024. Corresponding author: Y. Huang (e-mail: huangyk@seu.edu.cn).

Color versions of one or more figures in this article are available at https://doi.org/10.1109/TMAG.2023.3296718.

Digital Object Identifier 10.1109/TMAG.2023.3296718

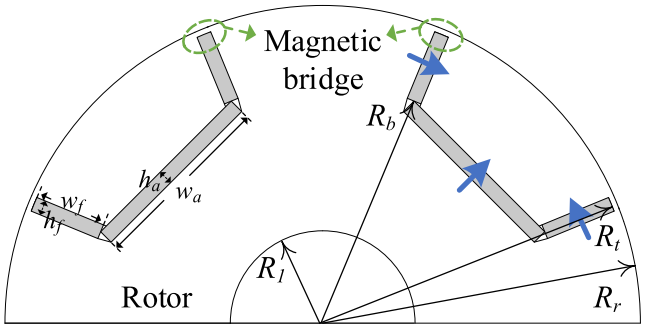

Fig. 1. Rotor structure of the studied motor.

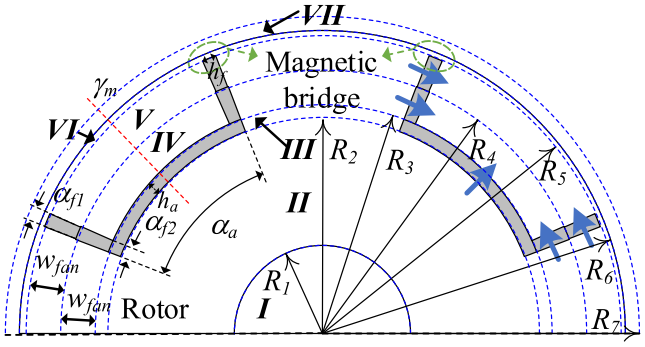

Fig. 2. Simplified rotor structure.

where k is the number of spoke-type fan-shaped PMs, in this article $k = 2$.

Then, the inner/outer radius and arc angle of each fan-shaped region can be obtained

$$R_4 = R_5 - w_{\text{fan}} = R_t - w_{\text{fan}} \tag{2}$$

$$R_3 = R_4 - w_{\text{fan}} = R_b \tag{3}$$

$$\alpha_{f1} = 2 \cdot \arcsin\left(\frac{h_f}{2 \cdot R_5}\right), \quad \alpha_{f2} = 2 \cdot \arcsin\left(\frac{h_f}{2 \cdot R_4}\right). \tag{4}$$

For the straight-shaped PM, the width is guaranteed to be h_a, and the equivalent fan-shaped region parameters are

$$R_2 = R_3 - h_a \tag{5}$$

$$\alpha_{fa} = 2 \cdot \arcsin\left(\frac{h_a}{2 \cdot R_2}\right). \tag{6}$$

The constant volume of the magnets is necessary to keep identical magnetic energy. Therefore, to compensate for the change in magnetic energy, it is necessary to introduce the area coefficient f_s

$$W_c = \frac{S_c L_{ef} B_{r,c}^2}{2\mu_r \mu_0}, \quad W_f = \frac{\sum_{k=1}^{K} S_f^k L_{ef} B_{r,f}^2}{2\mu_r \mu_0} \tag{7}$$

where S_c and S_f, $B_{r,c}$ and $B_{r,f}$ are the area and remanence density of cubic PM and fan-shaped PMs, respectively

$$S_f^{\text{III}} = \left(R_3^2 - R_2^2\right) \cdot \alpha_{fa} \tag{8}$$

$$S_f^{\text{IV}} = 2 \cdot \left(R_4^2 - R_3^2\right) \cdot \alpha_{f2} \tag{9}$$

$$S_f^{\text{V}} = 2 \cdot \left(R_5^2 - R_4^2\right) \cdot \alpha_{f1} \tag{10}$$

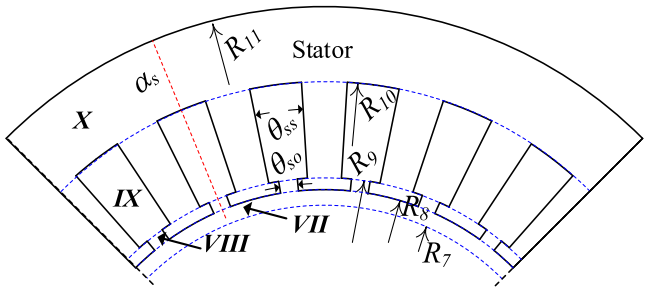

Fig. 3. Stator structure of the studied motor.

$$f_s = \frac{S_f}{S_c} = \frac{S_f^{\text{III}} + S_f^{\text{IV}} + S_f^{\text{V}}}{h_a \cdot w_a + 2 \cdot h_f \cdot w_f}. \tag{11}$$

Then, the equivalent remanence density $B_{r,f}$ of the fan-shaped PMs can be obtained as

$$B_{r,f} = (f_s)^{1/2} \cdot B_{r,c}. \tag{12}$$

The saturation effect of the magnetic bridge in the rotor core is the most obvious. In this article, the nonlinear iterative algorithm introduced in [8] and [9] is used to consider the nonlinear magnetic saturation of the magnetic bridges, and hence, is not repeated here. For the sake of simplicity, the rotor is segmented into two pieces: saturation region (i.e., magnetic bridge) and non-saturation region. The pole-arc angle of the magnetic bridge is simplified to α_{f1}.

The stator is divided into three simple computational regions (i.e., VIII, IX, X), as shown in Fig. 3.

III. Analytical Calculation

By introducing a magnetic vector potential A, the magnetic field in each region can be computed by solving the following Laplace's or Poisson's equations:

$$\frac{\partial^2 \boldsymbol{A}_z^k|_r}{\partial r^2} + \frac{1}{r}\frac{\partial \boldsymbol{A}_z^k|_r}{\partial r} - \left(\frac{\boldsymbol{V}^k}{r}\right)^2 \boldsymbol{A}_z^k|_r = -\boldsymbol{\mu}_{\boldsymbol{c},\boldsymbol{\theta}}^{\boldsymbol{k}} \boldsymbol{J}_z - \frac{\mu_0}{r}\left(\boldsymbol{M}_\theta^k + j\boldsymbol{K}_{\boldsymbol{\theta}} \boldsymbol{M}_r^k\right) \tag{13}$$

where

$$\boldsymbol{K}_{\boldsymbol{\theta}} = \text{diag}[-N, \ldots, N] \tag{14}$$

$$\boldsymbol{V}^k = \boldsymbol{\mu}_{c,\theta}^k \boldsymbol{K}_{\boldsymbol{\theta}} \left[\boldsymbol{\mu}_{c,r}^k\right]^{-1} \boldsymbol{K}_{\boldsymbol{\theta}}. \tag{15}$$

The general solution for each region is given as follows:

$$\boldsymbol{A}_z^k|_r = \begin{cases} \left(\frac{r}{R_1}\right)^{\lambda_1} \boldsymbol{a}_1, & k = I \\ \left[\left(\frac{R_{10}}{r}\right)^{\lambda_{10}} - \left(\frac{R_{10}}{R_{11}}\right)^{\lambda_{10}} \left(\frac{r}{R_{11}}\right)^{\lambda_{10}}\right] \boldsymbol{a}_{10}, & k = \text{X} \\ \boldsymbol{W}_k \left(\frac{r}{R_k}\right)^{\lambda_k} \boldsymbol{a}_{\boldsymbol{k}} + W_k \left(\frac{R_{k-1}}{r}\right)^{\lambda_k} \boldsymbol{b}_k & \\ \quad + r^2 \boldsymbol{F}_k + r \boldsymbol{G}_k, & k = \text{Others} \end{cases} \tag{16}$$

where

$$\boldsymbol{G}_k = \mu_0 \left(\left[\boldsymbol{V}^k\right]^2 - \boldsymbol{I}\right)^{-1} \left(\boldsymbol{M}_\theta^k + j\boldsymbol{K}_\theta \boldsymbol{M}_r^k\right), \quad k = \text{III, IV, V} \tag{17}$$

$$\boldsymbol{F}_k = \left(\left[\boldsymbol{V}^k\right]^2 - 4\boldsymbol{I}\right)^{-1} \boldsymbol{\mu}_{c,\theta}^k \boldsymbol{J}_z, \quad k = \mathrm{IX} \tag{18}$$

where $\boldsymbol{W}_k$ and $\boldsymbol{\lambda}_k$ are the diagonal eigenvalue and the eigenvector matrix of $\boldsymbol{V}^k$.

Based on the above general solutions, the interface continuity boundary conditions are listed as follows:

$$\boldsymbol{A}_z^k - \boldsymbol{A}_z^{k+1} = \boldsymbol{0}, \quad r = R_k \tag{19}$$

$$\boldsymbol{H}_\theta^k - \boldsymbol{H}_\theta^{k+1} = \boldsymbol{0}, \quad r = R_k. \tag{20}$$

All unknown harmonic coefficients and boundary conditions matrix equations are collected in the following matrix form:

$$\boldsymbol{M} \cdot \boldsymbol{X} = \boldsymbol{Y} \tag{21}$$

where $\boldsymbol{M}$, $\boldsymbol{X}$, and $\boldsymbol{Y}$ are the coefficient factors, the unknown coefficients, and the constant values in the boundary condition equations, respectively.

Then, according to the Maxwell stress tensor, the electromagnetic torque T_{em} can be obtained by

$$T_{\mathrm{em}} = \frac{L_{\mathrm{lef}} R_g^2}{\mu_0} \int_0^{2\pi} B_r^{\mathrm{VII}}(R_g, \theta) B_\theta^{\mathrm{VII}}(R_g, \theta) d\theta \tag{22}$$

where R_g, B_r^{VII}, and B_θ^{VII} are, respectively, the average radius, the radial, and tangential components of the no-load or on-load magnetic flux density in the air gap and L_{lef} is the active length of the motor.

The flux linkage of the ith coil could be computed by

$$\varphi_{1,i} = L_{\mathrm{lef}} \frac{N_c}{S} \int_{\alpha_i - \frac{\theta_{ss}}{2}}^{\alpha_i - \frac{\theta_{ss}}{2} + d} \int_{R_{st}}^{R_{sb}} A_z^{\mathrm{IV}}(r, \theta) dr d\theta \tag{23}$$

$$\varphi_{2,i} = L_{\mathrm{lef}} \frac{N_c}{S} \int_{\alpha_i + \frac{\theta_{ss}}{2} - d}^{\alpha_i + \frac{\theta_{ss}}{2}} \int_{R_{st}}^{R_{sb}} A_z^{\mathrm{IV}}(r, \theta) dr d\theta. \tag{24}$$

The total flux linkage per phase is given by

$$\begin{bmatrix} \Psi_a \\ \Psi_b \\ \Psi_c \end{bmatrix} = C_1 \begin{bmatrix} \varphi_{1,1} & \varphi_{1,2} & \cdots & \varphi_{1,Q_s} \end{bmatrix}^T + C_2 \begin{bmatrix} \varphi_{2,1} & \varphi_{2,2} & \cdots & \varphi_{2,Q_s} \end{bmatrix}^T. \tag{25}$$

Then, the three-phase back EMF can be derived as

$$\begin{bmatrix} E_a \\ E_b \\ E_c \end{bmatrix} = -\frac{d}{dt} \begin{bmatrix} \Psi_a \\ \Psi_b \\ \psi_c \end{bmatrix}. \tag{26}$$

For phase A, the machine is fed only by phase A with i_a, and the self- and mutual inductances can be calculated as follows:

$$\begin{bmatrix} L_a \\ M_{ab} \\ M_{ac} \end{bmatrix} = \begin{bmatrix} \Psi_a & \Psi_b & \Psi_c \end{bmatrix}^T / i_a. \tag{27}$$

IV. Results and Analysis

The developed analytical model can be used to predict the MFD in each calculation region and the EPs of the motor. The effectiveness of the proposed method is verified by the FE model, which is established by JMAG with 16 388 elements and 9344 nodes. In an entire electrical period, the FE model has 192 simulation steps.

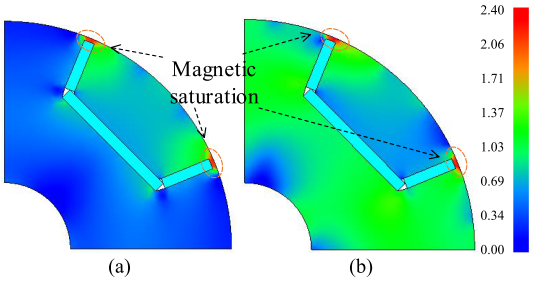

Fig. 4. FE models. (a) No-load condition. (b) On-load condition.

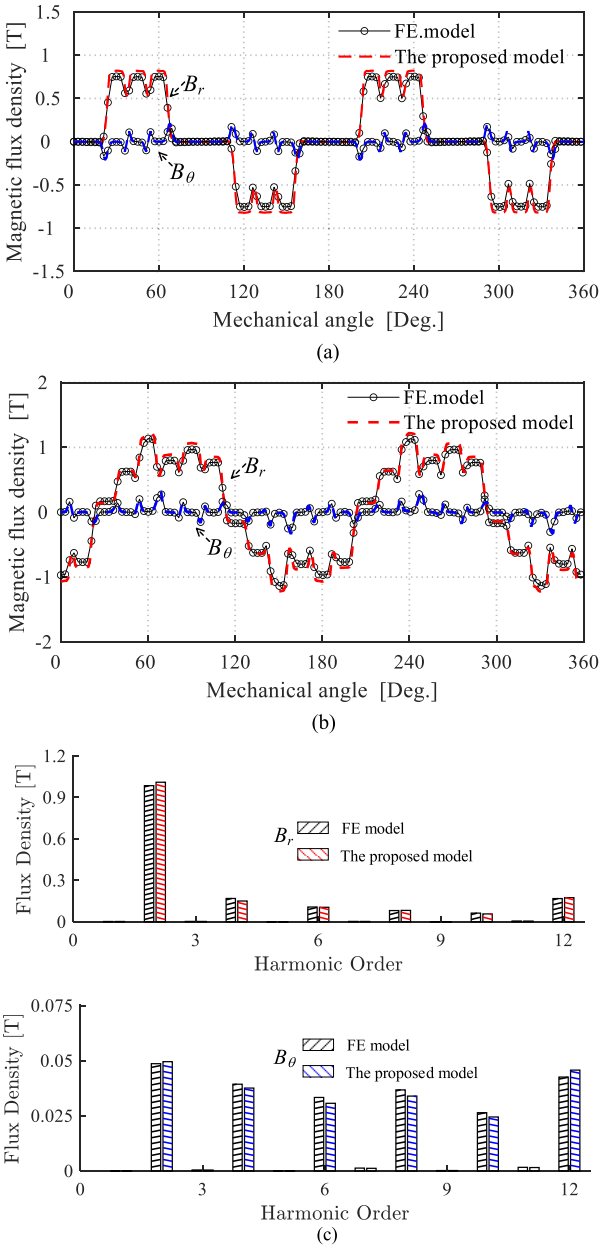

Fig. 5. Comparison of radial components of magnetic flux density in the air gap ($R_g = (R_6 + R_7)/2$). (a) Waveforms, no-load condition. (b) Waveforms, load condition. (c) Harmonic spectrum, load condition.

Fig. 4(a) and (b) show the MFD under no-load and load conditions respectively, it can be seen that the magnetic bridge has an obvious magnetic saturation phenomenon.

In Fig. 5(a) and (b), the comparison of the no-load and load air gap flux density components between the FE model

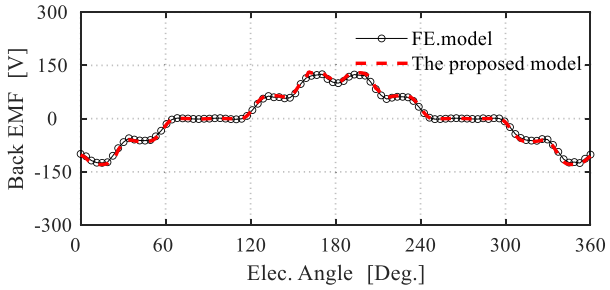

Fig. 6. Comparison of back EMF.

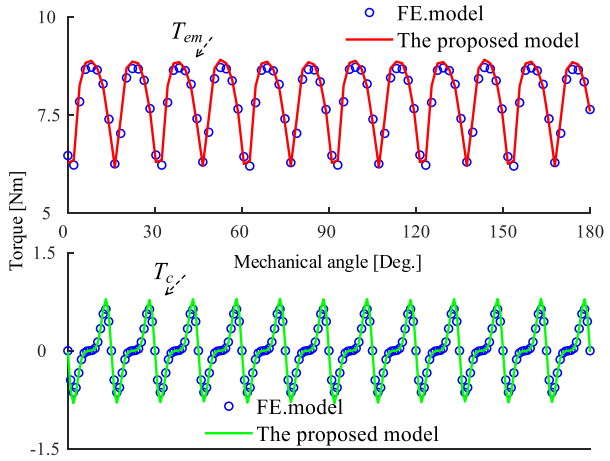

Fig. 7. Comparison of electromagnetic and cogging torques ($T_{\rm em}$ and T_c).

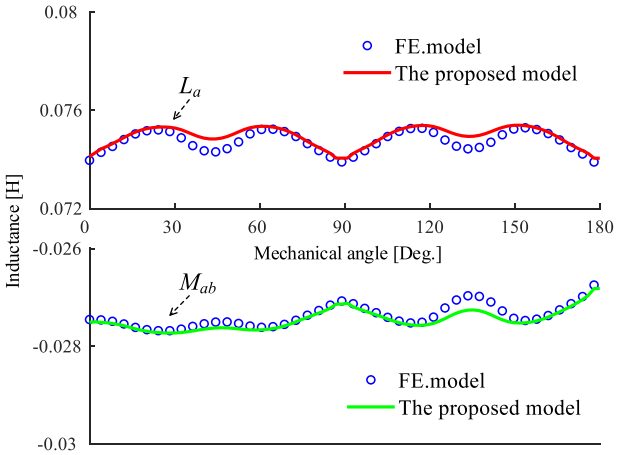

Fig. 8. Self-/mutual inductance (L_a and M_{ab}).

and the proposed model is given (B_r and B_θ are the radial and tangential components of the air gap flux density, respectively). It can be seen from the waveforms that the analytical results are in good agreement with the FE results. However, the spectrums (i.e., Fig. 5(c), load condition) show that there is a slight error in the amplitude of each harmonic order. This is due to the fact that the saturated region of the magnetic bridge is considered in the analytical model to be a regular region (i.e., the pole-arc angle is α_{f1}), whereas the saturated region of the rotor is irregular in the FE model, which results in a calculation error.

The back EMF waveform predicted by the proposed model is very consistent with the results of the FE model, as shown in Fig. 6. The calculated amplitude of the phase-back EMF is 131.9 V, while the FE model result is 127.8 V, and the relative error is only 3.2%.

Fig. 7 shows the comparison of electromagnetic torque $T_{\rm em}$ and cogging torque T_c. It is clear that the waveform predicted by the proposed model is very consistent with the FE analysis result.

Fig. 8 shows the comparison between the proposed model and the FE model for the variation of self- and mutual inductances with rotor position. The maximum and minimal values of the self-inductance are, respectively, $L_{a\max} = 0.0754$ H and $L_{a,\min} = 0.0741$ mH for the proposed model and $L_{a,\max} = 0.0753$ mH and $L_{a,\min} = 0.0738$ mH for the FE model.

V. Conclusion

This article presents a novel approach to predicting the magnetic field of U-shaped IPMMs. Specifically, each spoke-type PM is equivalent to two fan-shaped PMs, and the straight-shaped PM is equivalent to a fan-shaped PM with equal thickness. The saturated magnetic bridge is simplified to a standard fan-shaped region to consider the saturation effect of the magnetic bridge. Based on the HM technique, the phenomenon of nonuniform permeability distribution of the rotor ferromagnetic material due to magnetic saturation is directly taken into consideration. Moreover, with only small adjustments, the approach proposed in this article can be used to analyze Spoke or V-shaped IPMMs.

Acknowledgment

This work was supported in part by the National Natural Science Foundation of China under Grant 52277036.

References

[1] F. Liu, X. Wang, and Z. Xing, "Design of a 35 kW permanent magnet synchronous motor for electric vehicle equipped with non-uniform air gap rotor," *IEEE Trans. Ind. Appl.*, vol. 59, no. 1, pp. 1184–1198, Jan./Feb. 2023, doi: 10.1109/TIA.2022.3206258.

[2] B. Guo, Y. Huang, F. Peng, and J. Dong, "A new hybrid method for magnetic field calculation in IPMSM accounting for any rotor configuration," *IEEE Trans. Ind. Electron.*, vol. 66, no. 7, pp. 5015–5024, Jul. 2019, doi: 10.1109/TIE.2018.2868252.

[3] M. Hajdinjak and D. Miljavec, "Analytical calculation of the magnetic field distribution in slotless brushless machines with U-shaped interior permanent magnets," *IEEE Trans. Ind. Electron.*, vol. 67, no. 8, pp. 6721–6731, Aug. 2020, doi: 10.1109/TIE.2019.2939967.

[4] Y. An et al., "Open-circuit air-gap magnetic field calculation of interior permanent magnet synchronous motor with V-shaped segmented skewed poles using hybrid analytical method," *IEEE Trans. Magn.*, vol. 57, no. 12, pp. 1–9, Dec. 2021, doi: 10.1109/TMAG.2021.3118222.

[5] W. Liu, H. Yang, and H. Lin, "A hybrid field analytical method of hybrid-magnetic-circuit variable flux memory machine considering magnet hysteresis nonlinearity," *IEEE Trans. Transport. Electrific.*, vol. 7, no. 4, pp. 2763–2774, Dec. 2021, doi: 10.1109/TTE.2021.3085367.

[6] S. Li, W. Tong, M. Hou, S. Wu, and R. Tang, "Analytical model for no-load electromagnetic performance prediction of V-shape IPM motors considering nonlinearity of magnetic bridges," *IEEE Trans. Energy Convers.*, vol. 37, no. 2, pp. 901–911, Jun. 2022, doi: 10.1109/TEC.2021.3121438.

[7] R. L. J. Sprangers, J. J. H. Paulides, B. L. J. Gysen, and E. A. Lomonova, "Magnetic saturation in semi-analytical harmonic modeling for electric machine analysis," *IEEE Trans. Magn.*, vol. 52, no. 2, pp. 1–10, Feb. 2016, doi: 10.1109/TMAG.2015.2480708.

[8] Z. Djelloul-Khedda, K. Boughrara, F. Dubas, and R. Ibtiouen, "Nonlinear analytical prediction of magnetic field and electromagnetic performances in switched reluctance machines," *IEEE Trans. Magn.*, vol. 53, no. 7, pp. 1–11, Jul. 2017, doi: 10.1109/TMAG.2017.2679686.

[9] H. Zhao, C. Liu, Z. Song, and J. Yu, "A fast optimization scheme of coaxial magnetic gears based on exact analytical model considering magnetic saturation," *IEEE Trans. Ind. Appl.*, vol. 57, no. 1, pp. 437–447, Jan. 2021, doi: 10.1109/TIA.2020.3040142.